Spectrochimica Acta Part A: Molecular and Biomolecular Spectroscopy 137 (2015) 1174–1183

Contents lists available at ScienceDirect

Spectrochimica Acta Part A: Molecular and Biomolecular Spectroscopy

journal homepage: www.elsevier.com/locate/saa

Theoretical study of the structure–properties relationship in new class of 2,5-di(2-thienyl)pyrrole compounds

Sevgi Özdemir Kart [a,*], A. Ebru Tanboğa [a], Hakan Can Soyleyici [b], Metin Ak [c], Hasan Hüseyin Kart [a]

[a] Department of Physics, Faculty of Arts and Sciences, Pamukkale University, Kinikli, 20017 Denizli, Turkey
[b] Department of Chemistry, Faculty of Arts and Sciences, Adnan Menderes University, Aydın, Turkey
[c] Department of Chemistry, Faculty of Arts and Sciences, Pamukkale University, Kinikli, 20017 Denizli, Turkey

HIGHLIGHTS

- New class of 2,5-di(2-thienyl)pyrrole compound has been studied.
- The compound has been characterized by IR, ^{1}H and ^{13}C NMR spectroscopy.
- The results of HF and DFT/B3LYP methods are compatible with the measured results.

GRAPHICAL ABSTRACT

The monomer (HKCN) are characterized by IR, ^{1}H and ^{13}C NMR spectroscopy.

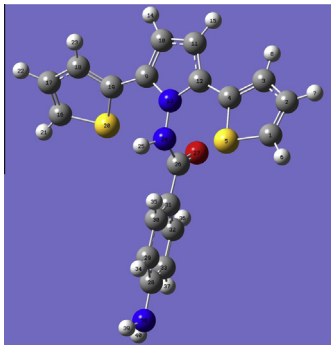

ARTICLE INFO

Article history:
Received 27 March 2014
Received in revised form 6 July 2014
Accepted 31 August 2014
Available online 22 September 2014

Keywords:
FT-IR
NMR
HF and DFT
Conducting polymer

ABSTRACT

Detailed studies of the structure–property relationships for conductive polymers are important for the proper understanding of the impact of morphological details on chemical and physical properties. This understanding is necessary for the development of realistic theoretical models. The particular cases of thienyl pyrroles are described. Ab initio methods based on Hartree–Fock (HF) and Density Functional Theory (DFT) calculations with the basis set of 6-31G(d) are performed to determine the molecular structural properties and to calculate FT-IR and NMR spectrum of the title molecule. Moreover, assignments of the vibrational modes are made on the basis of potential energy distribution (PED). Furthermore, the correlations between the observed and calculated frequencies are found to be in good agreement with each other as well as the correlation of the NMR data. A comparison of the experimental and theoretical calculations can be very useful in making correct assignment and understanding the properties and molecular structure relations.

Introduction

Conducting polymers (CPs) have been proposed for use in a wide variety of next generation technologies including electrochromic devices [1,2], organic photovoltaic devices [3], polymer light emitting diodes [4], non-linear optical devices [5], gas sensors [6], fuel cells [7,8] and organic transistors [9]. More recently, research on CPs has mostly focused on their optical properties in the visible and near infra-red (NIR) spectral regions. Polythiophene (PTh) derivatives have been the most studied materials since they exhibit fast switching times, high conductivity,

* Corresponding author.
E-mail address: ozsev@pau.edu.tr (S.Özdemir Kart).

http://dx.doi.org/10.1016/j.saa.2014.08.143
1386-1425/

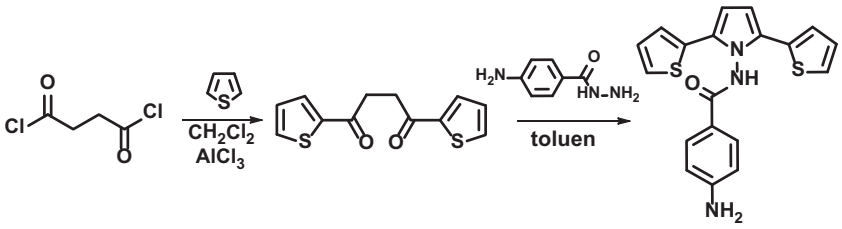

Scheme 1. Synthesis of the title molecule.

outstanding stability and high contrast ratios in the visible and NIR regions [10].

It is important to realize that structure plays a dominant role in determining the physical, electrical and optical properties of CPs [10–12]. Research has focused on directing the structure and function of these materials through synthesis. Synthesis can help to determine the magnitude of π overlap along the backbone and eliminate structural defects. Material assembly determines the interchain overlap and dimensionality. Planarization of the backbone and assembly of the backbone in the form of π stacks lead to better materials and device performance in almost every category, ranging from electrical conductivity to stability. The most striking conclusions are control of regularity and order in the polymeric structure, which leads to remarkable enhancements in the electronic and photonic properties of these materials [13]. This of course leads to the exciting prospect that the properties of polythiophenes can be selectively engineered through synthesis and assembly. A large portion of both the pioneering and future work

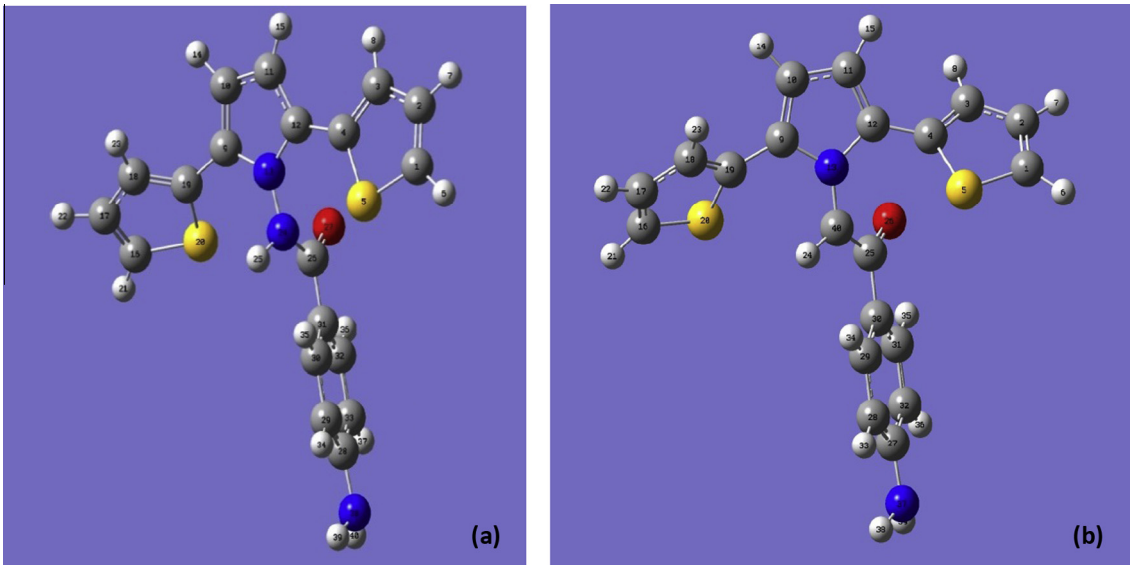

Fig. 1. The theoretical optimized molecular structures of the title molecule with (a) N—N bond and (b) N—C bond by utilizing DFT/B3LYP/6-31G(d) level. The C atom is substituted in place of N atom of the molecule with 24 atom number as shown in (a).

Table 1
Optical properties of same SNS derivatives in the literature.

Structure 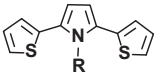		λ_{max}	E_g	%ΔT	Refs.
R1	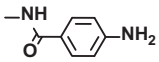	445	1.95	18 (440 nm)	[11]
R2	—H	410	2.88	–	[37]
R3	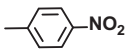	400	2.25	13 (400 nm)	[38]
R4		413	2.33	18 (423 nm)	[39]
R5	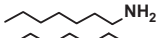	334	2.27	11 (334)	[10]
R6	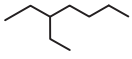	360	2.32	–	[40]

Table 2
The optimized geometrical parameters of the title molecule in the ground state employing DFT/B3LYP and HF methods with the basis set of 6-31G(d). Bond length in (Å), bond angles and dihedral angles in (°).

	Bond length via Gaussian (Å)	Symbolic bond labels (Å)	DFT/B3LYP/ 6-31G(d)	HF/6-31G(d)
1	R(1,2)	C1—C2	1.367	1.345
2	R(1,5)	C1—S5	1.736	1.724
3	R(1,6)	C1—H6	1.082	1.071
4	R(2,3)	C2—C3	1.422	1.434
5	R(2,7)	C2—H7	1.085	1.074
6	R(3,4)	C3—C4	1.380	1.350
7	R(3,8)	C3—H8	1.084	1.073
8	R(4,5)	C4—S5	1.758	1.740
9	R(4,12)	C4—C12	1.449	1.466
10	R(9,10)	C9—C10	1.386	1.358
11	R(9,13)	C9—N13	1.395	1.379
12	R(9,19)	C9—C19	1.453	1.467
13	R(10,11)	C10—C11	1.411	1.421
14	R(10,14)	C10—H14	1.081	1.071
15	R(11,12)	C11—C12	1.389	1.359
16	R(11,15)	C11—H15	1.081	1.071
17	R(12,13)	C12—N13	1.390	1.378
18	R(13,24)	N13—N24	1.377	1.361
19	R(16,17)	C16—C17	1.368	1.345
20	R(16,20)	C16—S20	1.733	1.723
21	R(16,21)	C16—H21	1.082	1.071
22	R(17,18)	C17—C18	1.424	1.433
23	R(17,22)	C17—H22	1.085	1.074
24	R(18,19)	C18—C19	1.379	1.352
25	R(18,23)	C18—H23	1.085	1.074
26	R(19,20)	C19—S20	1.760	1.741
27	R(24,25)	N24—H25	1.013	0.994
28	R(24,26)	N24—C26	1.405	1.372
29	R(26,27)	C26—O27	1.219	1.197
30	R(26,31)	C26—C31	1.487	1.489
31	R(28,29)	C28—C29	1.408	1.395
32	R(28,33)	C28—C33	1.409	1.397
33	R(28,38)	C228—N38	1.387	1.385
34	R(29,30)	C29—C30	1.389	1.380
35	R(29,34)	C29—H34	1.088	1.076
36	R(30,31)	C30—C31	1.404	1.391
37	R(30,35)	C30—H35	1.086	1.075
38	R(31,32)	C31—C32	1.404	1.392
39	R(32,33)	C32—C33	1.385	1.377
40	R(32,36)	C32—H36	1.085	1.073
41	R(33,37)	C33—H37	1.088	1.076
42	R(38,39)	N38—H39	1.011	0.996
43	R(38,40)	N38—H40	1.011	0.996
	Bond angles via Gaussian (°)	Symbolic bond angles (°)	DFT/B3LYP/ 6-31G(d)	HF/6-31G(d)
1	A(2,1,5)	C2—C1—S5	111.6	111.8
2	A(2,1,6)	C2—C1—H6	128.5	127.8
3	A(5,1,6)	S5—C1—H6	119.8	120.5
4	A(1,2,3)	C1—C2—C3	112.8	112.8
5	A(1,2,7)	C1—C2—H7	123.6	123.7
6	A(3,2,7)	C3—C2—H7	123.6	123.5
7	A(2,3,4)	C2—C3—C4	113.9	113.0
8	A(2,3,8)	C2—C3—H8	123.7	124.0
9	A(4,3,8)	C4—C3—H8	122.4	123.0
10	A(3,4,5)	C3—C4—S5	109.8	110.9
11	A(3,4,12)	C3—C4—C12	125.5	129.1
12	A(5,4,12)	S5—C4—C12	124.6	120.0
13	A(1,5,4)	C1—S5—C4	91.9	91.6
14	A(10,9,13)	C10—C9—N13	106.4	107.3
15	A(10,9,19)	C10—C11—C19	128.3	128.4
16	A(13,9,19)	N13—C9—C19	125.2	124.2
17	A(9,10,11)	C9—C10—C11	108.5	107.8
18	A(9,10,14)	C9—C10—H14	124.5	125.1
19	A(11,10,14)	C11—C10—H14	127.0	127.0
20	A(10,11,12)	C10—C11—C12	108.4	107.8
21	A(10,11,15)	C10—C11—H15	126.7	126.9
22	A(12,11,15)	C12—C11—H15	125.0	125.3
23	A(4,12,11)	C4—C12—C11	128.1	129.4
24	A(4,12,13)	C4—C12—N13	125.4	123.3
25	A(11,12,13)	C11—C12—N13	106.4	107.4
26	A(9,13,12)	C9—N13—C12	110.4	109.6
27	A(9,13,24)	C9—N13—N24	125.8	124.9
28	A(12,13,24)	C12—N13—N24	123.7	124.4
29	A(17,16,20)	C17—C16—S20	111.8	112.2
30	A(17,16,21)	C17—C16—H21	128.3	127.6
31	A(20,16,21)	S20—C16—H21	119.9	120.2
32	A(16,17,18)	C16—C17—C18	112.7	112.3
33	A(16,17,22)	C16—C17—H22	123.5	123.9
34	A(18,17,22)	C18—C17—H22	123.8	123.8
35	A(17,18,19)	C17—C18—C19	113.8	113.4
36	A(17,18,23)	C17—C18—H23	124.1	123.9
37	A(19,18,23)	C19—C18—H23	122.1	122.7
38	A(9,19,18)	C9—C19—C18	125.7	125.4
39	A(9,19,20)	C9—C19—S20	124.3	123.8
40	A(18,19,20)	C18—C19—S20	109.9	110.6
41	A(16,20,19)	C16—S20—C19	91.8	91.5
42	A(13,24,25)	C13—N24—H25	114.7	115.6
43	A(13,24,26)	C13—N24—C26	119.7	121.4
44	A(25,24,26)	H25—N24—C26	119.3	120.6
45	A(24,26,27)	N24—C26—O27	121.2	122.0
46	A(24,26,31)	N24—C26—C31	115.0	115.1
47	A(27,26,31)	O27—C26—C31	123.9	122.9
48	A(29,28,33)	C29—C28—C33	118.5	118.7
49	A(29,28,38)	C29—C28—N38	120.7	120.6
50	A(33,28,38)	C33—C28—N38	120.7	120.6
51	A(28,29,30)	C28—C29—C30	120.6	120.4
52	A(28,29,34)	C28—C29—H34	119.5	119.7
53	A(30,29,34)	C30—C29—H34	119.9	119.9
54	A(29,30,31)	C29—C30—C31	121.0	121.1
55	A(29,30,35)	C29—C30—H35	118.4	118.3
56	A(31,30,35)	C31—C30—H35	120.6	120.6
57	A(26,31,30)	C26—C32—C30	124.4	123.9
58	A(26,31,32)	C26—C31—C32	117.3	117.8
59	A(30,31,32)	C30—C31—C32	118.2	118.3
60	A(31,32,33)	C31—C32—C33	121.2	121.1
61	A(31,32,36)	C31—C32—H36	118.2	118.8
62	A(33,32,36)	C33—C32—H36	120.6	120.1
63	A(28,33,32)	C28—C33—C32	120.5	120.4
64	A(28,33,37)	C28—C33—H37	119.4	119.6
65	A(32,33,37)	C32—C33—H37	120.0	120.0
66	A(28,38,39)	C28—N38—H39	116.4	115.7
67	A(28,38,40)	C28—N38—H40	116.3	115.6
68	A(39,38,40)	H39—N38—H40	112.8	112.1
	Dihedral angles via Gaussian (°)	Symbolic dihedral angles (°)	DFT/B3LYP/ 6-31G(d)	HF/6-31G(d)
1	D(5,1,2,3)	S5—C1—C2—C3	0.2	0.5
2	D(5,1,2,7)	S5—C1—C2—H7	−178.8	179.8
3	D(6,1,2,3)	H6—C1—C2—C3	178.0	−179.3
4	D(6,1,2,7)	H6—C1—C2—H7	−1.0	0.0
5	D(2,1,5,4)	C2—C1—S5—C4	−0.4	−0.5
6	D(6,1,5,4)	H6—C1—S5—C4	−178.3	179.3
7	D(1,2,3,4)	C1—C2—C3—C4	0.1	−0.2
8	D(1,2,3,8)	C1—C2—C3—H8	−179.0	178.3
9	D(7,2,3,4)	H7—C2—C3—C4	179.1	−179.5
10	D(7,2,3,8)	H7—C2—C3—H8	0.0	−1.0
11	D(2,3,4,5)	C2—C3—C4—S5	−0.4	−0.1
12	D(2,3,4,12)	C2—C3—C4—C12	175.7	178.5
13	D(8,3,4,5)	H8—C3—C4—S5	178.7	−178.6
14	D(8,3,4,12)	H8—C3—C4—C12	−5.3	0.0
15	D(3,4,5,1)	C3—C4—S5—C1	0.4	0.3
16	D(12,4,5,1)	C12—C4—S5—C1	− 175.7	−178.4
17	D(3,4,12,11)	C3—C4—C12—C11	−17.2	−128.0
18	D(3,4,12,13)	C3—C4—C12—C13	162.6	51.8
19	D(5,4,12,11)	S5—C4—C12—C11	158.3	50.5
20	D(5,4,12,13)	S5—C4—C12—N13	−21.9	−129.6
21	D(13,9,10,11)	N13—C9—C 10—C11	0.1	−0.4
22	D(13,9,10,14)	N13—C9—C10—H14	179.1	177.5
23	D(19,9,10,11)	C19—C9—C10—C11	175.8	176.8
24	D(19,9,10,14)	C19—C9—C10—H14	−5.2	−5.2
25	D(10,9,13,12)	C10—C9—N13—C12	−0.2	0.6
26	D(10,9,13,24)	C10—C9—N13—N24	178.0	169.4
27	D(19,9,13,12)	C19—C9—N13—C12	−176.1	−176.8
28	D(19,9,13,24)	C19—C9—N13—N24	2.2	−8.0
29	D(10,9,19,18)	C10—C9—C19—C 18	−39.1	−51.2
30	D(10,9,19,20)	C 10—C9—C 19—S20	135.4	124.0

Table 2 (*continued*)

	Bond length via Gaussian (Å)	Symbolic bond labels (Å)	DFT/B3LYP/ 6-31G(d)	HF/6-31G(d)
31	D(13,9,19,18)	N13—C9—C19—C18	135.8	125.6
32	D(13,9,19,20)	N13—C9—C19—S20	−49.7	−59.1
33	D(9,10,11,12)	C9—C10—C11—C12	0.1	0.0
34	D(9,10,11,15)	C9—C10—C11—H15	−179.3	177.6
35	D(14,10,11,12)	H14—C10—C11—C12	−178.9	−177.9
36	D(14,10,11,15)	H14—C10—C11—H15	1.7	−0.3
37	D(10,11,12,4)	C10—C11—C12—N13	179.7	−179.8
38	D(10,11,12,13)	C10—C11—C12—N13	−0.2	0.3
39	D(15,11,12,4)	H15—C11—C12—C4	−1.0	2.6
40	D(15,11,12,13)	H15—C11—C12—N13	179.2	−177.3
41	D(4,12,13,9)	C4—C12—N13—C9	−179.6	179.5
42	D(4,12,13,24)	C4—C12—N13—N24	2.1	10.7
43	D(11,12,13,9)	C11—C12—N13—C9	0.3	−0.6
73	D(11,12,13,24)	C11—C12—C13—N24	−178.0	−169.4
74	D(9,13,24,25)	C9—N13—N24—H25	−65.6	−67.1
75	D(9,13,24,26)	C9—N13—N24—C26	86.3	95.5
76	D(12,13,24,25)	C12—C13—N24—H25	112.4	100.0
77	D(12,13,24,26)	C12—N13—N24—C26	−95.6	−97.3
78	D(20,16,17,18)	S20—C16—C17—C18	−1.1	−0.5
79	D(20,16,17,22)	S20—C16—C17—H22	−180.0	−180.0
80	D(21,16,17,18)	H21—C16—C17—C18	178.3	179.2
81	D(21,16,17,22)	H21—C16—C 17—H22	−0.5	−0.3
82	D(17,16,20,19)	C17—C16—S20—C19	1.3	0.6
83	D(21,16,20,19)	H21—C16—S20—C19	−178.2	−179.1
84	D(16,17,18,19)	C16—C17—C18—C 19	0.2	0.1
85	D(16,17,18,23)	C16—C17—C18—H23	−178.4	−179.5
86	D(22,17,18,19)	H22—C17—C18—C19	179.1	179.5
87	D(22,17,18,23)	H22—C17—C18—H23	0.4	−0.1
88	D(17,18,19,9)	C17—C18—C19—C9	175.9	176.2
89	D(17,18,19,20)	C17—C18—C 19—S20	0.7	0.4
90	D(23,18,19,9)	H23—C18—C19—C9	−5.4	−4.2
91	D(23,18,19,20)	H23—C18—C 19—S20	179.4	−180.0
92	D(9,19,20,16)	C9—C19—S20—C 16	−176.4	−176.5
93	D(18,19,20,16)	C18—C19—S20—C16	−1.1	−0.6
94	D(13,24,26,27)	N13—N24—C26—O27	4.2	1.8
95	D(13,24,26,31)	N13—N24—C26—C31	−176.4	−178.7
96	D(25,24,26,27)	H25—N24—C26—O27	154.9	163.6
97	D(25,24,26,31)	H25—N24—C26—C31	−25.7	−16.9
98	D(24,26,31,30)	N24—C26—C31—C30	−17.0	−25.5
99	D(24,26,31,32)	N24—C26—C31—C32	163.8	156.3
100	D(27,26,31,30)	O27—C26—C31—C30	162.4	154.1
101	D(27,26,31,32)	O27—C26—C31—C32	−16.7	−24.1
102	D(33,28,29,30)	C33—C28—C29—C30	0.6	0.8
103	D(33,28,29,34)	C33—C28—C29—H34	−178.4	−178.2
104	D(38,28,29,30)	N38—C28—C29—C30	177.6	178.1
105	D(38,28,29,34)	N38—C28—C29—H34	−1.3	−0.9
106	D(29,28,33,32)	C29—C28—C33—C32	−0.3	−0.2
107	D(29,28,33,37)	C29—C28—C33—H37	179.3	179.1
108	D(38,28,33,32)	N38—C28—C33—C32	−177.4	−177.6
109	D(38,28,33,37)	N38—C28—C33—H37	2.2	1.8
110	D(29,28,38,39)	C29—C28—N38—H39	23.6	24.9
111	D(29,28,38,40)	C29—C28—N38—H40	160.3	158.8
112	D(33,28,38,39)	C33—C28—N38—H40	−159.4	−157.9
113	D(33,28,38,40)	C33—C28—N38—H40	−22.7	−24.0
114	D(28,29,30,31)	C28—C29—C30—C31	0.1	−0.1
115	D(28,29,30,35)	C28—C29—C30—H35	−177.7	−178.0
116	D(34,29,30,31)	H34—C29—C30—C31	179.0	178.8
117	D(34,29,30,35)	H34—C29—C30—H35	1.2	0.9
118	D(29,30,31,26)	C29—C30—C31—C26	179.8	−179.2
119	D(29,30,31,32)	C29—C30—C31—C32	−1.0	−1.0
120	D(35,30,31,26)	H35—C30—C31—C26	−2.4	−1.4
121	D(35,30,31,32)	H35—C30—C31—C32	176.7	176.8
122	D(26,31,32,33)	C26—C31—C32—C33	−179.5	179.9
123	D(26,31,32,36)	C26—C31—C32—H36	0.3	−0.3
124	D(30,31,32,33)	C30—C31—C32—C33	1.3	1.6
125	D(30,31,32,36)	C30—C31—C32—H36	−178.9	−178.6
126	D(31,32,33,28)	C31—C32—C33—C28	−0.6	−0.9
127	D(31,32,33,37)	C31—C32—C33—H37	179.8	179.7
128	D(36,32,33,28)	H36—C32—C33—C28	179.6	179.3
129	D(36,32,33,37)	H36—C32—C33—H37	0.0	−0.1

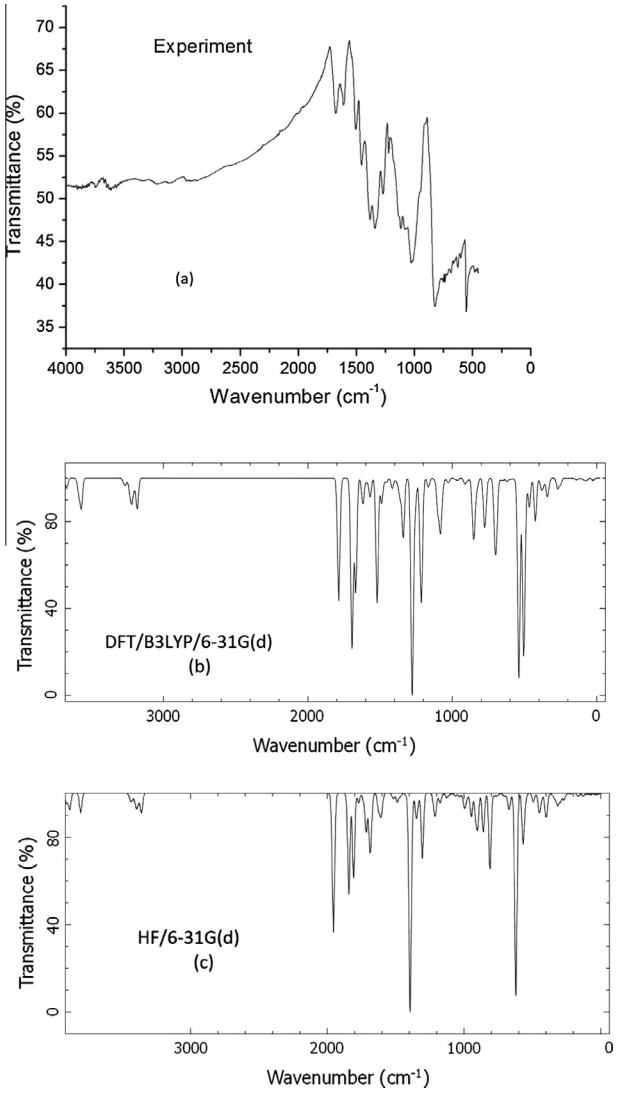

Fig. 2. (a) Experimental, (b) and (c) the calculated infrared spectra (FT-IR) of the title molecule by using DFT/B3LYP and HF methods with the 6-31G(d) basis set, respectively.

in conjugated polymers strongly depends on synthetic chemists creating new polymers that can be fabricated into new devices and whose physics and chemistry can be understood in detail [14].

The theoretical studies on the chemical compounds provide us to get the important information about the physical and chemical properties of them. For example, vibrational spectroscopy is a versatile and readily available tool for interpreting and predicting the properties of chemically and biologically active molecules. It has been used both in the study of chemical kinetics and chemical analysis. However, the problem of vibrational mode assignment as well as the understanding of the relationship between the observed spectroscopic properties and the molecular structure may be difficult [15]. Advances in ab initio computational chemistry help us to solve this problem accurately. Ab initio computations in chemistry are important tools to predict the structural properties of the molecules and to determine the vibrational spectra of ones. Recently, DFT and HF methods are widely used to determine the molecular structures and vibrational spectra for medium and large sized molecules at low computational cost [16–26]. These

computation methods generally give systematic errors mainly due to limited basis sets, harmonic approximation and remaining deficiencies in describing electron correlation [27]. In order to overcome these errors some theoretical methods have been used for fitting of calculated vibrational frequencies to experimentally observed ones. The studies on chemical shift calculations utilizing quantum chemistry methods show that the geometry optimization of the molecule is an important factor for accurate determination of NMR chemical shifts [28].

Both of experimental studies and theoretical calculations on the structural and vibrational properties of the title molecule are scarcity in the literature. Therefore, in order to comprehend and understand the structural and spectroscopic properties of the title molecule it is needed to be carried out further theoretical and experimental studies aiming to describe the fundamental properties of it. Ab initio methods based on the quantum mechanics in the computational chemistry are widely used to investigate some physical and chemical properties of the materials and chemical compounds [29,30].

2,5-Di(2-thienyl)pyrroles (SNS) that are very important class of monomers for the synthesis of conductive polymer in the literature consist of thiophene and pyrrole rings interconnected by their α-positions and are undoubtedly of interest in the preparation from them of electroconductive materials, in particular as components of smart devices. In a large number of the papers aimed at investigation of N-substituted 2,5-di(2-thienyl)pyrroles the Paal–Knorr synthesis, where the main starting compound is 1,4-di(2-thienyl)-1,4-butanedione in reaction with the respective amines, is used for the production of these triheterocycles [10,11].

New class 2,5-Di(2-thienyl)pyrrole derivative is synthesized via reaction with 1,4-di(2-thienyl)-1,4-butanedione and p-aminobenzoyl hydrazide. Using hydrazide instead of amine is not only increase product yield but also improve properties of the corresponding polymer [11]. In the present work, we have reported theoretical characterization and molecular structure of the title molecule by using the ab initio methods based on DFT and HF levels. Early experimental studies show that title compounds have superior properties compared with other thienyl pyrrole compounds [11]. Thus, conclusion of this article can be useful for designing of the new thienyl pyrrole monomers. A comparison of the experimental and theoretical calculations can be very useful in making correct assignment and understanding the basic vibrational, NMR spectra and molecular structure relations. In other words, a discussion on the experimental and theoretical studies of this compound leads to a better understanding of the nature of title compound. And so, these calculations are valuable for providing insight into design of new conducting polymers that used in technological applications.

The rest of the paper is organized as follows: experimental details and some results are presented in Section 'Experimental'. The computational method is given in Section 'Computational details'. The simulation results for structural and vibrational properties for the title molecule considered in this study are presented and discussed in Section 'Results and discussion'. The simulation

Table 3
The observed FT-IR and the calculated vibrational wavenumbers for the title molecule calculated from the DFT/B3LYP and HF levels with basis set of 6-31G(d) in the unit of cm^{-1}. IR intensities (km mol^{-1}) and assignments with PED (obtained from DFT/B3LYP/6-3G(d)) percentage in the brackets. Scale factors are used as 0.9614 and 0.8953 for the DFT/B3LYP and HF methods with 6-31G(d) basis set, respectively.

Mode no	DFT/B3LYP/6-31G(d)			HF/6-31G(d)			Experimental	Assignment [PED] > 10% [a]
	Unscaled	Scaled	I^{IR}	Unscaled	Scaled	I^{IR}		
1	3670	3528	14.02	3907	3498	20.23	3876	νNH(100)
2	3586	3447	19.17	3884	3477	32.55	3737	νNH(100)
3	3568	3430	38.75	3804	3406	39	3567	νNH(100)
7	3261	3135	6.31	3429	3070	10.69	3067	νCH(99)
15	3180	3057	18.25	3358	3006	18.4	2780	νCH(99)
16	1787	1718	161.42	1955	1750	277.11	1679	νOC(85)
18	1669	1605	149.22	1807	1618	167.02	1611	νCC(27) + δHNH(12)
22	1572	1511	9.07	1736	1554	12.04	1541	νCC(50)
25	1521	1462	161.22	1679	1503	50.21	1504	δHNC(59)
26	1490	1432	31.49	1626	1455	30.9	1455	νCC(53)
29	1456	1400	5.30	1597	1430	6.7	1382	νNN(23) + δCNC(26)
31	1397	1343	1.37	1508	1350	0.33	1340	νCC(11) + δHCS(10)
35	1348	1296	8.35	1418	1270	6.03	1272	νCC(10) + δHCC(50)
42	1213	1166	148.94	1305	1168	129.36	1272	δHCC(71)
44	1125	1081	1.41	1220	1092	11.04	1118	δHCS(26) + δHCC(32)
45	1117	1074	0.09	1213	1086	7.86	1084	δHCS(46) + δHCC(32)
53	982	944	1.11	1106	991	2.42	1028	τHCCC(70) + τCCCC(16)
57	911	876	1.16	1032	924	6.83	825	τHCSC(12) + τHCCC(78)
61	854	821	1.91	974	872	2.42	825	τHCCC(42) + τHCCN(28)
69	776	746	2.34	859	769	73.58	825	τHCCC(85)
70	769	739	27.38	849	760	7.23	752	τHCCC(34) + τHCCN(41)
71	745	716	0.09	811	726	70.83		νNN(11)
72	739	711	0.47	809	725	65.99	752	γONCC(42) + γNCCC(11) + γCCCC(14)
73	707	680	28.77	808	723	6.25	738	νSC(37) + δCCC(41)
78	653	628	0.70	710	635	4.05	665	τHCSC(54) + τHCCC(10)
82	594	571	1.36	661	592	5.81	629	δSCC(52)
83	581	559	0.35	636	570	8.62	602	δOCN(18) + δCCC(20)
84	565	543	2.09	621	556	397.53	602	δSCC(11) + τCCCC(34)
86	507	487	206.39	568	508	98.4	555	δSCC(10) + δCNN(14) + τCCCC(19)
87	499	479	37.66	552	494	16.4	555	τHNCC(41) + γNCCC(19)
89	467	449	38.57	493	441	17.43	482	τSCCC(48)
90	425	409	55.63	460	412	2.61	482	τSCCC(59)
97	331	318	0.57	335	300	10.38	453	τHNCC(91)

[a] PED: potential energy distribution. ν; stretching. δ; in-plane-bending. γ; out-of plane bending. τ; torsion.

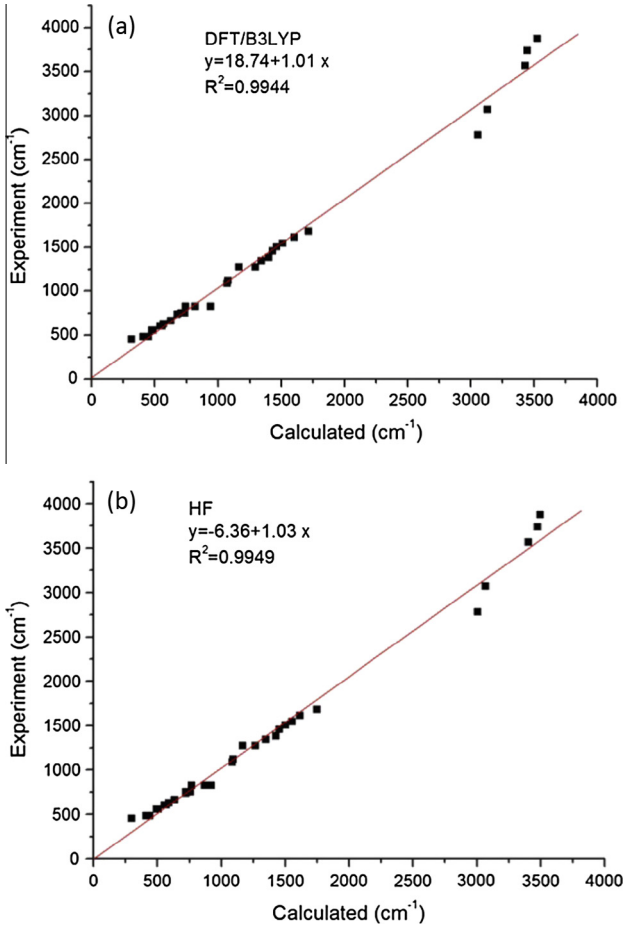

Fig. 3. The correlation graphs between the experimental and calculated wavenumber for the title molecule calculated from (a) DFT/B3LYP/6-31G(d) and (b) HF/6-31G(d) levels, respectively.

results are also compared with the available experimental data in Section 'Results and discussion'. Finally, the conclusions arising from our main results are given in the last section.

Experimental

Materials

Aluminum chloride ($AlCl_3$) (Aldrich), dichloromethane (DCM) (Merck), succinyl chloride (Aldrich), hydrochloric acid (Merck), $NaHCO_3$ (Aldrich), $MgSO_4$ (Aldrich), propionic acid (Aldrich), toluene (Sigma), acetonitrile (AN) (Merck) are commercially available and used without further purification.

Equipments

NMR spectrum of the monomer is recorded on a Bruker-Instruments-NMR Spectrometer (DPX-400) using $CDCl_3$ as the solvent. The FTIR spectra are recorded on a Varian 1000 spectrometer.

Synthesis of monomer

The reagents 1,4-di(2-thienyl)-1,4-butanedione and p-aminobenzoyl hydrazide are prepared according to the methods as given in the literature [31,32]. All experiments are carried out under dry argon by using Standard Schlenk techniques. Solvents are dried, distilled and saturated with argon.

The monomer (HKCN) is synthesized from 1,4-di(2-thienyl)-1,4-butanedione and p-aminobenzoyl hydrazide in the presence of catalytically amount of p-toluenesulphonic acid (PTSA) [11]. A round-bottomed flask equipped with an argon inlet and magnetic stirrer is charged with 2.5 g (10 mmol) 1,4-di(2-thienyl)-1,4-butanedione, 1.51 g (10 mmol) p-aminobenzoyl hydrazide, 0.2 g (1.2 mmol) PTSA, 1 ml DMSO and 20 ml toluene. The resultant mixture is stirred and refluxed for 18 h under argon. Darkened solution is filtered hot to remove oily decomposition products. Then, the mixture is cooled to room temperature and the solid product is filtered off to give a yellow powder that is washed with pentane (3 × 15 ml) and air-dried, yield 3.1 g%85, (mp 142–143 °C) [11]. The synthetic route of the monomer is shown in Scheme 1.

Computational details

To provide complete information regarding to the structural characteristic and the fundamental vibrational modes of the title molecule we have performed quantum mechanical calculations with the Gaussian 09 package by using the DFT/B3LYP/6-31G(d) and HF/6-31G(d) methods [33,34]. Molecular structure is optimized to get the global minima of the molecule at the level of ab initio DFT/B3LYP and HF with the basis set of 6-31G(d) by considering C1-symmetry (no symmetry constraint).

The optimized geometric molecular structures of the molecules with N—N bond and C—N bond are given in Fig. 1(a) and (b). After that, the same basis set and computational method are used for the vibrational spectra of it by using the optimized structure. The same calculation procedure is also used to predict the ^1H and ^{13}C NMR shielding constants by applying the Gauge-Including Atomic Orbitals (GIAO) GIAO-DFT and GIAO-HF methods [34] in the medium of dimethylsulfoxide (DMSO). The calculation for ^1H chemical shift is achieved by using the integral equation formalism version of the polarizable continuum model (IEFPCM). The stability of the optimized geometries is verified by wavenumbers calculations giving no negative values for all the calculated wavenumbers. VEDA 4 (Vibrational Energy Distribution Analysis) program [35] has been used to calculate Potential Energy Distribution (PED) for each of the vibrational frequencies. PED calculations show the relative contribution of the redundant internal coordinates to each normal vibrational mode of the molecule and thus it allows ones to describe the character of each mode numerically. The fundamental vibrational modes are characterized by their PEDs for the assignments of the experimental bands in details. The harmonic frequencies obtained from ab initio methods are multiplied by the appropriate scaled factors [36] to compare with the experimental frequencies. The incomplete incorporation of electron correlation and the use of finite basis set in the ab initio calculations lead to some systematic errors. Therefore, we have used the scaled factors as 0.9614 and 0.8953 for DFT/B3LYP and HF methods [36], respectively, in order to determine the vibrational spectra of the molecule accurately. The values of the vibrational modes corresponding to optimized geometry of the title molecule calculated by DFT and HF methods.

Results and discussion

Molecular geometry and structural properties

One principal goal of condensed matter theory is to understand the structure–property relationship of materials systems such that specific materials properties may be achieved via molecular design. The emergence of fascinating applications using π-conjugated polymers in light-emitting devices, electrochromic devices and photovoltaics requires precise control and flexible tuning of optical

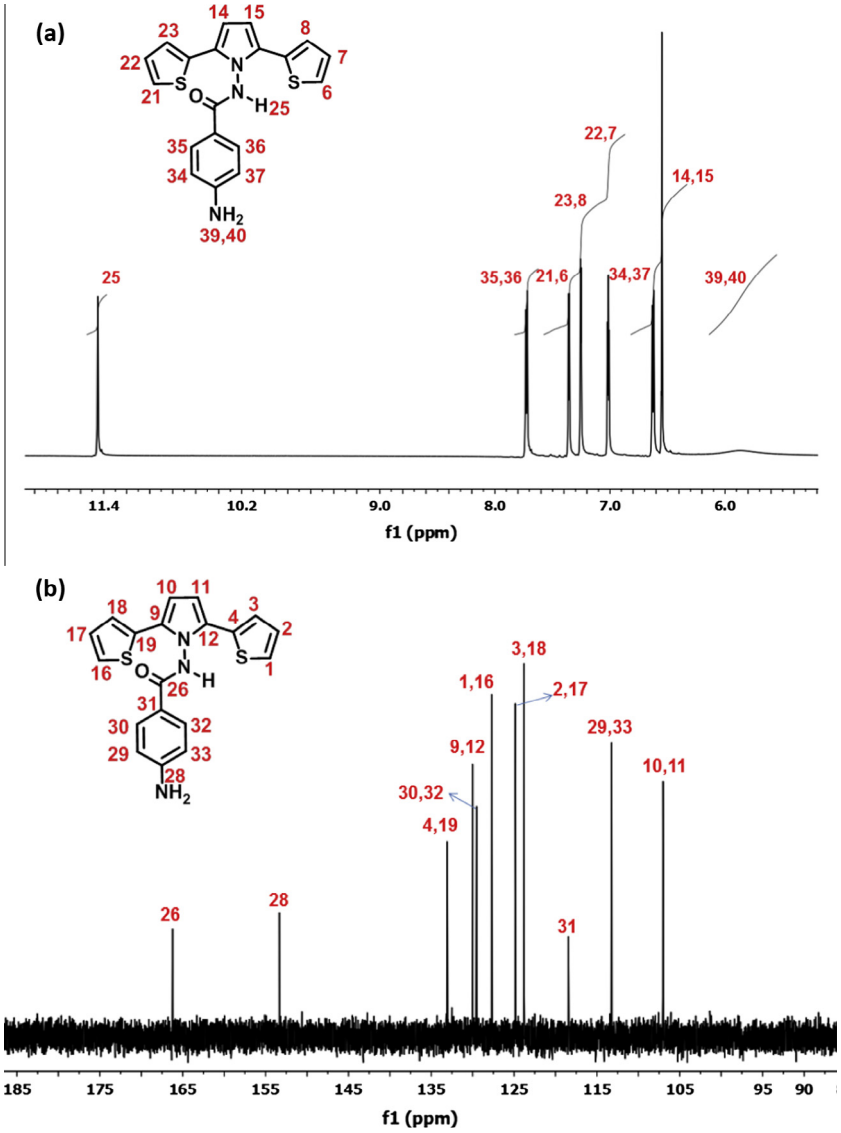

Fig. 4. (a) ^{1}H NMR spectrum of the title molecule and (b) ^{13}C NMR spectrum of the title molecule.

bandgaps to effectively cover the visible and other parts of the solar spectrum. The optical bandgap of organic molecules can be qualitatively derived from its dependence on the bond length alternation pattern, planarity, aromaticity, and/or electron-withdrawing/releasing substitutions [13]. Although useful in describing certain trends, these properties are ultimately dependent on the electronic structure of the molecule, which must hence be incorporated in any accurate quantitative description.

2,5-Di(2-thienyl)pyrroles (SNS) consist of thiophene and pyrrole rings interconnected by their α-positions and are undoubtedly of interest in the preparation from them of electro conductive materials, in particular as components of smart devices. But SNS derivatives generally have large band gap which is greater than 2 eV, low π–π* transition wavelength which is nearly in UV region and low optical contrast at π–π* transition wavelength. Experimental studies on our new title SNS compound show that has superior optic and electronic properties when compared with other SNS derivatives [11]. To explain these properties, we have investigated optimized geometric structures of title compound obtained from DFT/B3LYP/6-31G(d) level.

The optimized geometric structures obtained from DFT/B3LYP/6-31G(d) level and the atom numbering schemes of the title molecule with N—N bond and C—N bond are represented in Fig. 1(a) and (b), respectively. Theoretical analysis has shown that presence of N bond instead of C bond to thienyl pyrrole group in molecule is forced to structural planarity as seen in Fig. 1. Planarity contributes delocalization of π-electrons along the consecutive units and hence to decrease band gap. Having more planar structure, title compound has lower band gap and has better optical properties compared with other SNS derivatives. Table 1 shows optical and electronic properties of some SNS derivatives in the literature.

The geometry of the title molecule possesses C_1 point group symmetry. This molecule has 40 atoms and has got 114 fundamental vibrational modes. The main structural difference of the title molecule with other thienyl pyrrole monomers is presence of the N—N bond instead of C—N bond.

Another specificity of polyaromatic systems concerns the rotational disorder around interannular single bonds. A mean dihedral angle between consecutive units thus contributes to limit the delocalization of π-electrons along the conjugated backbone and hence to increase band gap. The optimized structural parameters such as bond length, bond angle and dihedral angle of the title molecule determined from DFT/B3LYP and HF levels by using 6-31G(d) basis

Table 4
The experimental and theoretical ^{1}H and ^{13}C NMR chemical shifts (with respect to TMS) for the title molecule in the medium of DMSO (all values in ppm).

Atom (indices)	Experiment	Calculations	
		DFT/B3LYP/6-31G(d)	HF/6-31G(d)
H39 (a)	5.81	3.10	2.75
H40 (a)	5.81	3.08	2.76
H34 (b)	6.59	6.17	6.38
H37 (b)	6.59	6.26	6.64
H35 (c)	7.67	7.22	7.38
H36 (c)	7.67	7.54	8.26
H25 (d)	11.40	6.44	5.88
H6 (e)	7.31	6.59	7.12
H21 (e)	7.31	6.66	7.11
H7 (f)	6.97	6.59	6.83
H22 (f)	6.97	6.60	6.85
H8 (g)	7.21	6.88	6.92
H23 (g)	7.21	6.61	6.98
H14 (h)	6.50	6.03	6.21
H15 (h)	6.50	6.18	6.13
C28 (a)	152.92	136.59	152.01
C29 (b)	112.81	99.98	106.37
C33 (b)	112.81	100.57	107.70
C30 (c)	129.60	114.60	130.01
C32 (c)	129.60	118.82	134.17
C31 (d)	118.03	106.36	112.92
C26 (e)	165.82	152.36	163.88
C1 (f)	127.28	116.05	127.85
C16 (f)	127.28	118.56	129.75
C2 (g)	124.43	111.47	121.60
C17 (g)	124.43	111.81	120.68
C4 (i)	132.67	124.98	132.67
C19 (i)	132.67	125.15	132.41
C9 (j)	132.10	116.54	126.39
C12 (j)	132.10	118.05	126.84
C10 (k)	106.61	97.95	105.48
C11 (k)	106.61	93.53	104.22
C3 (h)	123.39	108.79	123.19
C18 (h)	123.39	113.66	126.84

Labels of the atoms in this Table are given according to Fig. 1(a) used in the assignment of the chemical shifts.

set are presented in Table 2. In order to define the molecular structure of the title molecule 43 bond lengths, 68 bond angles and 129 dihedral angles are necessary. These bond lengths, bond angles and dihedral angles are given in Table 2.

Rotational disorder around interannular single bonds in molecule as seen in Fig. 1(b) contributes to the delocalization of π-electrons along the conjugated backbone and hence to decrease band gap.

Analysis of vibrational spectra

Vibrational spectroscopy is one of the most useful tools for characterization of the chemical compounds in terms of both experimental studies and theoretical calculations. In this present study, we have performed a frequency calculation analysis to obtain the spectroscopic signature of the title molecule. The experimental FT-IR spectra of the title molecule and their corresponding theoretical calculations of FT-IR spectra computed from DFT/B3LYP and HF methods with basis set of 6-31G(d) are plotted in Fig. 2(a)–(c), respectively. Some specific and important vibrational modes of the theoretical data computed from DFT and HF methods are given in Table 3 along with the assignment of fundamental vibration modes. The experimental results are also given in Table 3 to compare them with the corresponding theoretical results. All the theoretical vibrational wavenumbers, IR intensity calculations predicted from DFT/B3LYP/6-31G(d) and HF/6-31G(d) and assignments of IR vibration modes of the title molecule are provided in Table S1 as a Supplementary material. Of the 114 normal modes of the vibrations, 39 modes are stretching vibration, 38 are bending modes of the vibrations and the remaining 37 modes are torsional vibrational. This molecule has 36 CH vibrational modes.

It is important to deal with the some fundamental vibrational modes observed in the material studied in this work. For example, the bands of the N—H stretching vibrations are observed at the wavenumbers of 3876 cm^{-1}, 3737 cm^{-1} and 3567 cm^{-1} while the theoretical scaled values of N—H vibrations are predicted as 3528 cm^{-1}, 3447 cm^{-1} and 3430 cm^{-1} by using DFT/B3LYP/6-31G(d), respectively. They are also calculated as 3498 cm^{-1}, 3447 cm^{-1} and 3406 cm^{-1} via the HF/6-31G(d).

The C—H stretching vibrations of aromatic and heteroaromatic structures are normally found in the region of 3000–3100 cm^{-1} [41]. They are observed at the 2780 cm^{-1} and 3067 cm^{-1}. The scaled streching C—H vibrations in the ranges of 3148–3059 cm^{-1} and 3009–3083 cm^{-1} are calculated by using DFT/B3LYP/6-31G(d) and HF/6-31G(d) methods, respectively. From Table 3, the theoretically calculated results scaled down corresponding with C—H stretching vibrations show good agreement with the experimentally observed vibrations.

In case of O=C stretching vibration, a very strong band at 1679 cm^{-1} in FT-IR spectra is attributed the O=C stretching vibration, which is in agreement with the scaled results at 1718 cm^{-1} (for DFT/6-31G(d)) and 1750 cm^{-1} (for HF/6-31G(d)).

There is one stretching vibration at 1611 cm^{-1} in the FT-IR spectrum, assigned to C=C stretching vibration. The value for C=C stretching vibration is calculated at 1605 cm^{-1} and 1618 cm^{-1} by using DFT/B3LYP/6-31G(d) and HF/6-31G(d) methods, respectively.

The mainly carbon–carbon vibrations modes named as stretching, in-plane-bending, out-of plane bending and torsion occur in the region of 1611–453 cm^{-1}. The vibrational data calculated from DFT and HF methods with the basis set of 6-31G(d) are compatible with the corresponding observed values of the FT-IR. The other observed vibrations of the title molecule are also given in Table 3. It is to say that it is difficult to assign all bands due to the complexity of the vibration bands. Therefore, it is shown that only characteristic vibration bands can be identified.

The correlation graphs of the calculated versus experimental vibrational frequencies for the title molecule are given in Fig. 3(a) and (b) predicted from DFT and HF levels, respectively. Linear regression is carried out by using the linear equation of $y = A + Bx$, where A and B are fit constants. The correlation between the experimental and the calculated frequencies after scaling are linear as shown in Fig. 3(a) and (b). The equalities; $y = 18.74 + 1.01x$ ($R^2 = 0.9944$) and $y = 6.36 + 1.03\ x$ ($R^2 = 0.9949$) are obtained by using the methods of DFT/B3LYP and HF, respectively. It can be concluded that the frequency values obtained from the methods of DFT/B3LYP and HF are consistent with the experimental data since the slope and the intercept values in the case of both methods go to unity and zero, respectively, as shown in Fig. 3.

NMR spectra

The characterization of the title molecule is further clarified by the use of ^{1}H and ^{13}C NMR spectroscopy. The ^{1}H and ^{13}C NMR spectra of the title molecule are recorded in the medium of dimethylsulfoxide (DMSO). The experimentally observed ^{1}H and ^{13}C NMR spectra of title molecule (with respect to TMS, and in DMSO solution) are shown in Fig. 4(a) and (b), respectively. ^{1}H NMR (400 MHz, 25 °C, in DMSO-d_6 = 11.40δ (s; $1H^{d=25}$, —NH—), 7.67δ (d; $2H^{c=35,36}$), 7.31δ (d; $2H^{e=6,21}$), 7.21δ (d; $2H^{g=8,23}$), 6.97δ (t; $2H^{f=7,22}$), 6.59δ (d; $2H^{b=34,37}$), 6.50δ (s; $2H^{h=14,15}$) 5,81δ (br. s; $2H^{a=39,40}$, —NH_2). In the ^{1}H NMR spectra of HKCN the resonance of the NH proton appears as a singlet at 11.40 ppm. The broad absorption peak appeared at 5.81 ppm is assigned to the NH_2 protons of benzene ring. The signal of the aromatic atoms of the

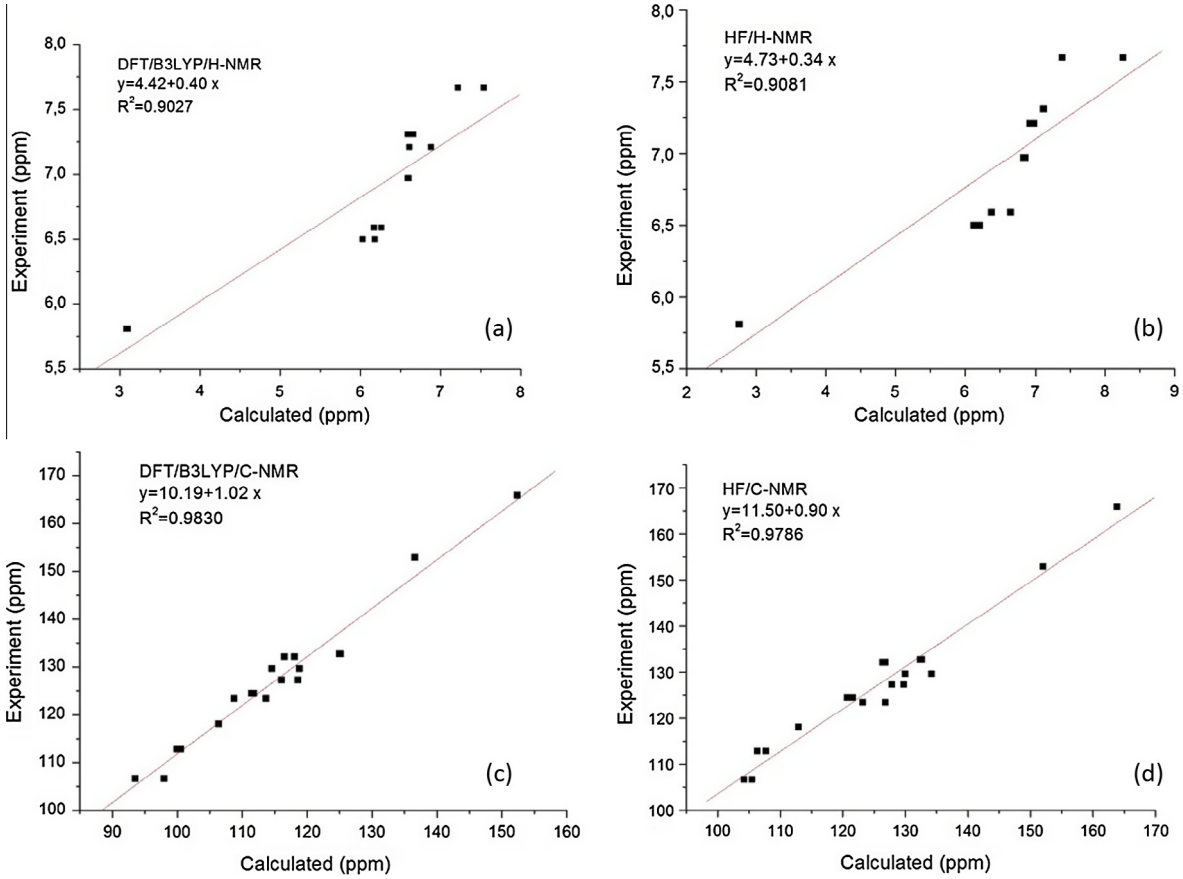

Fig. 5. The correlation graphs between the experimental and theoretical ^{1}H and ^{13}C NMR chemical shift values of the title molecule calculated from DFT/B3LYP/6-31G(d) and HF/6-31G(d) levels as shown in (a), (b), (c) and (d), respectively.

phenyl group gives two duplets at 6.59 and 7.69 ppm. The signal of the aromatic atoms of the thienyl groups gives three peaks in the interval 6.50–6.97 ppm and the aromatic pyrrole protons gives singlet at 6.50 ppm.

^{13}C NMR (400 MHz, 25 °C, in DMSO-d6) = 165.82, 152.92, 132.67, 132.10, 129.60, 127.28, 124.43, 123.39, 118.03, 112.81, 106.61. The ^{13}C NMR spectrum of HKCN give four signals (a = 28, b = 29,33, c = 30,32, d = 31) for the aromatic C atoms of the phenyl groups, six signals (f = 1,16, g = 2,17, h = 3,18, i = 4,19, j = 9,12, k = 10,11) for the aromatic C atoms of pyrrolyl and thienyl groups in the interval 106.61–152.92 ppm and one signal (e = 26) for carbonyl groups at 165.82 ppm [11] as seen in Fig. 4(b).

In addition, GIAO ^{1}H and ^{13}C chemical shift calculations with respect to TMS are carried out by using the DFT/B3LYP and HF with the basis set of 6-31G(d) in the medium of dimethylsulfoxide (DMSO) for the optimized structure. The results of these calculations are given in Table 4 for the ^{1}H and ^{13}C chemical shift values of the optimized title molecule with the available experimental data. We have investigated the correlation between the calculation and experiment to compare the computed and experimental NMR data. The linear correlation coefficients (R^2) are obtained by using the experimental ^{1}H and ^{13}C NMR chemical shift values and the data for DFT/B3LYP and HF methods except for the data of 25-H. The graphs of the linear correlation of ^{1}H and ^{13}C for DFT/B3LYP and HF methods with the basis set of 6-31G(d) are given in Fig. 5(a)–(d), respectively. According to the these correlation values the agreement (R^2 = 0.9081) between the experimental and calculated ^{1}H chemical shifts for the HF level is good in the solvent of DMSO. However, the correlation (R^2 = 0.9830) between the measured and computed ^{13}C chemical shift for the DFT/B3LYP method is also in good agreement in the solvent of DMSO. It can be said that both methods, DFT and HF, compute the compatible chemical shift values of ^{1}H and ^{13}C for the title molecule.

Conclusion

In this study, DFT and ab initio HF calculations for the title molecule are presented for the first time in this work. The geometry of the title molecule is optimized by using the DFT/B3LYP and HF levels with the basis set of 6-31G(d). The complete molecular structural parameters such as bond lengths, bond angles and dihedral angles have been computed by utilizing these methods. Moreover, the vibrational frequencies of the fundamental modes of the title molecule have been precisely assigned and analyzed and the computed results have been compared with the experimental vibrational frequencies. The observed and calculated fundamental frequencies by using DFT/B3LYP and HF with 6-31G(d) basis set show similar profiles in both position and intensities making normal modes assignment. The harmonic frequencies calculated from ab initio methods based on quantum mechanics deviate from the frequencies, slightly. The observed disagreement between the theoretical and the experimental results could be a consequence of the anharmonicity and of the general tendency of the quantum chemical methods to overestimate of the force constants at the exact equilibrium geometry. The best correlation equalities for the IR; $y = 18.74 + 1.01x$ (R^2 = 0.9944) and $y = 6.36 + 1.03\ x$ (R^2 = 0.9949) are obtained by using the methods of DFT/B3LYP and HF, respectively. Moreover, linear regression (R^2 = 0.9081) between the experimental and calculated ^{1}H chemical shifts for the HF level is good in the solvent of DMSO. Additionally, the correlation

(R^2 = 0.9830) between the measured and computed ^{13}C chemical shift for the DFT/B3LYP method is compatible with each other. It can be said that both methods compute the compatible chemical shift values of ^{1}H NMR and ^{13}C NMR of the molecule. Theoretical analysis has shown that presence of N bond instead of C bond to thienyl pyrrole group is forced to structural planarity. Rotational order around interannular single bonds contributes to the delocalization of π-electrons along the conjugated backbone and hence to decrease band gap. Having more planar structure, title compound has lower band gap and has better optical properties compared with other SNS derivatives.

Acknowledgements

This study has been supported by Pamukkale University (Grant Nos: 2013FBE009, 2013FBE013) and TUBITAK (Grant No: 101T074).

Appendix A. Supplementary material

Supplementary data associated with this article can be found, in the online version, at http://dx.doi.org/10.1016/j.saa.2014.08.143.

References

[1] I. Yağmur, M. Ak, A. Bayrakçeken, Smart Mater. Struct. 22 (2013) 115022.
[2] M. Ak, M.S. Ak, M. Güllü, L. Toppare, Smart Mat. Struct. 16 (2007) 2621–2626.
[3] D. Hazar Apaydın, D.E. Yildiz, A. Cirpan, L. Toppare, Sol. Energy Mat. Sol. Cells 113 (2013) 100–105.
[4] P.J. Skabara, Chem. Commun. 49 (2013) 9242–9244.
[5] M. Boussouale, R.C.Y. King, J. -F Brun, B. Duponchel, M. Ismaili, F. Roussel, J. Appl. Phys. 108 (2010) 113526.
[6] M. Ak, B. Yigitsoy, Y. Yagci, L. Toppare, E-Polym. 7 (2007) 495–502.
[7] F. Memioğlu, A. Bayrakçeken, T. Öznülüer, M. Ak, Int. J. Energy Res. 37 (2012) 16673–16679.
[8] F. Memioğlu, A. Bayrakçeken, T. Öznülüer, M. Ak, Int. J. Energy Res. (2014), http://dx.doi.org/10.1002/er.3126.
[9] S.M. Islam, P. Banerji, S. Banerjee, Org. Electron. 15 (2014) 144–149.
[10] S. Tarkuc, M. Ak, E. Onurhan, L. Toppare, J. Macromol. Sci. Pure Appl. Chem. 45 (2008) 164–171.
[11] H.C. Söyleyici, M. Ak, Y. Şahin, D.O. Demikol, S. Timur, Mat. Chem. Phys. 142 (2013) 303–310.
[12] M. Içli-Özkut, H. Ipek, B. Karabay, A. Cihaner, A.M. Önal, Polym. Chem. 4 (2013) 2457–2463.
[13] J. Roncali, Macromol. Rapid Commun. 28 (2007) 1761–1775.
[14] J. Liu, D. Haynes, C. Balliet, R. Zhang, T. Kowalewski, R.D. McCullough, Adv. Funct. Mater. 22 (2012) 1024–1032.
[15] V. Krishnakumar, R.J. Xavier, T. Chithambarathanu, Spectrochim. Acta Part A Mol. Biomol. Spectrosc. 62 (2005) 931–939.
[16] M. Karabacak, E. Sahin, M. Cinar, I. Erol, M. Kurt, J. Mol. Struct. 886 (2008) 148–157.
[17] X. Xuan, J. Wang, Y. Zhao, J. Zhu, J. Raman Spectrosc. 38 (2007) 865–872.
[18] M. Karabacak, A. Coruh, M. Kurt, J. Mol. Struct. 892 (2008) 125–131.
[19] N. Sundaraganesen, C. Meganathan, B.D. Joshua, P. Mani, A. Jayaprakash, Spectrochim. Acta Part A Mol. Biomol. Spectrosc. 71 (2008) 1134–1139.
[20] N. Sundaraganesen, C. Meganathan, B.D. Joshua, Spectrochim. Acta Part A Mol. Biomol. Spectrosc. 69 (2008) 871–879.
[21] X. Xuan, C. Zhai, Spectrochim. Acta A 79 (2011) 1663–1668.
[22] M.R. Anoop, P.S. Binil, S. Suma, M.R. Sudarsnakumar, S. Mary, Y.H.T. Vaghese, C. Yohannan Panicker, J. Mol. Struct. 969 (2010) 48–54.
[23] A. Atac, M. Karabacak, C. Karaca, E. Köse, Spectrochim. Acta Part A Mol. Biomol. Spectrosc. 85 (2012) 145–154.
[24] M. Karabacak, Z. Cinar, M. Kurt, S. Sudha, N. Sundaraganesan, Spectrochim. Acta Part A Mol. Biomol. Spectrosc. 85 (2012) 179–189.
[25] P.B. Nagabalasubramanian, M. Karabacak, S. Periandy, Spectrochim. Acta Part A Mol. Biomol. Spectrosc. 85 (2012) 43–52.
[26] M. Kurt, T.R. Sertbakan, M. Ozduran, M. Karabacak, J. Mol. Struct. 921 (2009) 178–187.
[27] S. Katsyuba, E. Vandyukova, Chem. Phys. Lett. 377 (2003) 658–662.
[28] J. Casanovas, A.M. Namba, S. Leon, G.L.B. Aquino, D.V.J. da Silva, C. Aleman, J. Org. Chem. 66 (2001) 3775–3782.
[29] H. Chermette, Coord. Chem. Rev. 178–180 (1998) 699–721.
[30] C. Corminboeuf, F. Tran, J. Weber, J. Mol. Struct: THEOCHEM 672 (2006) 1–7.
[31] P.E. Just, K.I. Chane-Ching, P.C. Lacaze, Tetrahedron 58 (2002) 3467–3472.
[32] R. Gup, E. Giziroglu, Spectrochim. Acta A 65 (2006) 719–726.
[33] J.B. Foresman, A.E. Frisch, Exploring Chemistry with Electronic Structure Methods, Gaussian Inc., 1996.
[34] M.J Frisch et al., Gaussian 09, Revision A.1, Gaussian Inc., Wallingford CT, 2009.
[35] M.H. Jamroz, Vibrational Energy Distribution Analysis: VEDA 4 Program, Warsaw, 2004.
[36] A.P. Scott, L. Radon, J. Phys. Chem. 100 (1996) 16502–16513.
[37] G. Gordon, M.G.B. McLeod, M. Jones, A. Richard, S.D. Watson, N.D. Truong, J.C. Galin, J. François, Polymer 27 (1986) 455–458.
[38] S. Varis, M. Ak, C. Tanyeli, I.M. Akhmedov, L. Toppare, Eur. Polym. J. 42 (2006) 2352–2360.
[39] A. Cihaner, F. Algı, J. Electroanal. Chem. 614 (2008) 101–106.
[40] P. Camurlu, C. Gültekin, Z. Bicil, Electrochim. Acta 61 (2012) 50–56.
[41] L.J. Bellamy, The Infrared Spectra of Complex Molecules, John Wiley, New York, 1956.